Available online at www.sciencedirect.com
SCIENCE DIRECT
Acta Materialia 54 (2006) 2813–2821
Acta MATERIALIA
www.actamat-journals.com

Effects of crystal structure and grain orientation on the roughness of deformed polycrystalline metals

O. Wouters, W.P. Vellinga, R. van Tijum, J.Th.M. De Hosson *

Department of Applied Physics, Materials Science Centre and the Netherlands Institute for Metals Research, University of Groningen, Nijenborgh 4, 9747 AG Groningen, The Netherlands

Received 7 October 2005; received in revised form 1 February 2006; accepted 16 February 2006
Available online 24 April 2006

Abstract

Surface roughening during tensile deformation of polycrystalline aluminum, iron and zinc is investigated using white light confocal microscopy and orientation imaging microscopy. A height–height correlation technique is used to analyze the data. The surface obeys self-affine scaling on length scales up to a correlation length which approximately equals the grain size and above which no height correlation is present. The self-affine scaling exponent increases initially with strain and saturates at a value around 0.9 for aluminum and at 0.8 for iron and zinc. A linear relation is observed between root mean square roughness and strain. The observed grain scale roughening is explained as arising from orientation differences between neighboring grains and depends on the available number of slip systems in the material. Orientation imaging microscopy is used to investigate the influence of the orientation of the surface grains and subsurface grains on the topography. It is found that the Schmid factor of surface grains alone is not enough to predict local deformation and evolution of surface height. In particular, grains with high Schmid factor may show less deformation than expected. It is shown that subsurface grains influence the roughness and it is hypothesized that a high cumulative Schmid factor on a cross-section below a point at the surface leads to a depression at the surface.

Keywords: Orientation imaging microscopy; Surface structure; Tension test; Mesostructure

1. Introduction

The roughness of a metal surface determines, sometimes even to a large extent, important properties such as reflectivity, lubricant transport, weldability and adhesion of surface layers. A rough surface may also facilitate the creation of initiation sites for strain localization, which may seriously degrade the mechanical properties of a material. Roughness originates when the metal is plastically deformed, e.g. in industrial rolling or forming processes. As a consequence, the roughening process has been the subject of numerous investigations, including both experimental and modeling studies [1–9].

In a recent paper, we used a statistical method for roughness analysis [1]. By calculating height–height correlations and comparing these to the results expected for a surface obeying self-affine scaling behavior over a limited range of scales, three parameters can be deduced. The use of these parameters, being the root mean square (rms) roughness w, the self-affine scaling exponent α and the correlation length ξ, offers insight into the roughness characteristics at different length scales. It was found that for a polycrystalline Al–Mg alloy the roughness on length scales below the correlation length ξ could be described by a high self-affine scaling exponent ($\alpha \sim 0.9$) and above the correlation length by an rms roughness, which increases linearly with strain and grain size. The latter is in accordance with earlier findings [8,9]. By performing straining experiments on different specimens of the same material but with different grain sizes, it was found that there is a linear relation

* Corresponding author.
E-mail address: j.t.m.de.hosson@rug.nl (J.Th.M. De Hosson).

1359-6454/$30.00
doi:10.1016/j.actamat.2006.02.023

between correlation length and area averaged grain size and that the correlation length is in fact almost equal to the grain size.

This clearly different behavior on scales below and above the grain size of a material suggests that the large-scale roughness is dominated by the differences between individual grains. Since in these experiments no other differences between the grains are present apart from their crystal orientation with respect to the tensile axis, it is assumed that these differences in hardness, causing strain incompatibilities between neighboring grains, are the source of the roughness.

In this paper, we concentrate on the role of the grain orientation in surface roughening. This is done by repeating the previous measurements for different materials with different crystal structures and by combining roughness measurements with information provided by orientation imaging microscopy (OIM).

2. Experimental

2.1. Materials and preparation

To examine the effect of the crystal structure, in addition to face-centered cubic (fcc) aluminum, materials with body-centered cubic (bcc) and hexagonal close-packed (hcp) crystal structures were chosen. The aluminum alloy used is Al–8.5% Mg. This alloy was selected because, due to the high solubility of magnesium in aluminum, the solid solution strengthening will guarantee sufficient toughness. It is believed that no secondary phases will be present in the bulk of the (large) grains although some precipitation may have occurred on grain boundaries. Furthermore, after a considerable amount of cold rolling (~80%), a recrystallization treatment at different temperatures and for different times offers the possibility of obtaining a large range of grain sizes without a significant texture. The bcc material is 3 N pure iron and is here assumed to deform plastically as pure iron would. It was cold rolled to 40% and recrystallized for 30 min at 800 °C to obtain a grain size comparable to the aluminum specimens. The hcp material selected is 5 N pure zinc, cold rolled to 50% and recrystallized for 30 min at 220 °C. Before each new step in the cold rolling process, the specimens were rotated by 90° in order to minimize the occurrence of texture upon recrystallization.

A summary of all the materials and treatments used is given in Table 1. Inverse pole figures are shown in Fig. 1 for the iron and zinc materials. Insets show the (1 1 1) and the (0 0 0 1) pole figures as well as grain size distributions for both materials. The figures show that the grains are fairly uniformly shaped and not strongly textured. Table 1 shows grain sizes obtained from OIM scans of an area of 800 μm × 800 μm. The grain sizes were determined by calculating the area-averaged diameter $\bar{d}$ from the area-averaged area $\overline{A}_A$:

$$\bar{d} = \sqrt{\frac{4\overline{A}_A}{\pi}} \quad \text{with } \overline{A}_A = \sum_{i=1}^{N} a_i A_i, \tag{1}$$

where N is the number of grains not touching the edges of the OIM scan, A_i is the area and a_i is the area fraction of grain i. In Table 1 the asymmetry of the distribution

Table 1
Summary of the materials used

Material	Structure	Heat treatment	$\bar{d}$ (μm)	$\bar{d}/\bar{d}_N$
Al–8.5% Mg	fcc	30 min, 350 °C	28	1.3
		30 min, 400 °C	49	2.1
		10 min, 450 °C	73	3.3
		30 min, 450 °C	97	4.4
Iron	bcc	30 min, 800 °C	34	1.5
Zinc	hcp	30 min, 220 °C	57	2.1

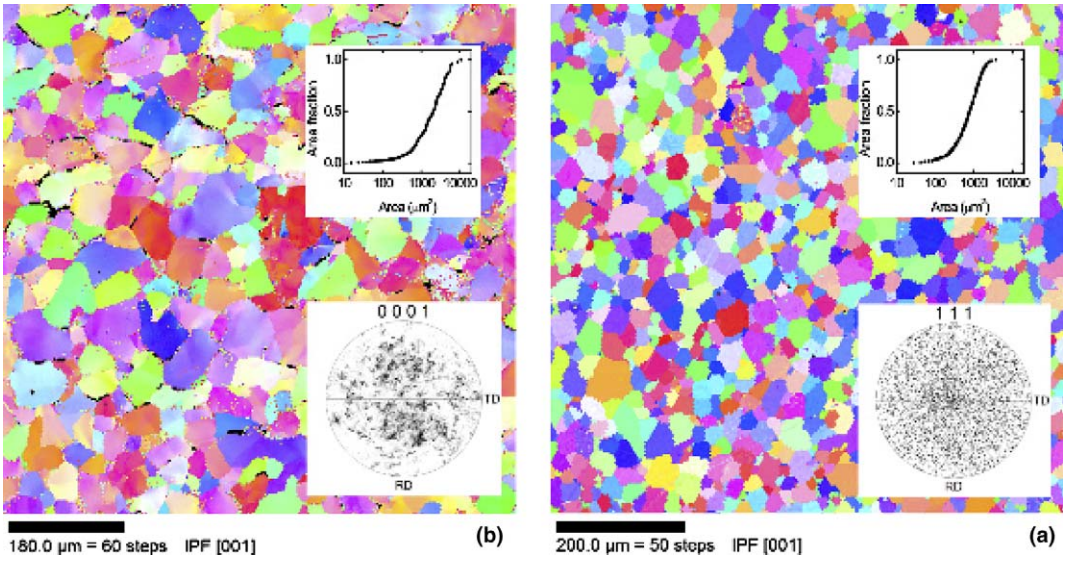

Fig. 1. Inverse pole figures for (a) iron sample and (b) zinc sample. The insets show, respectively, the (1 1 1) and (0 0 0 1) pole figures.

functions is further characterized by the ratio $\bar{d}/\bar{d}_N$ with $\bar{d}_N$ being the diameter calculated from the number-averaged area. Results for the aluminum specimens are qualitatively similar (see Ref. [1] and Table 1).

2.2. Experimental setup

From the materials described above, long flat tensile specimens were spark cut eroded with gauge dimensions of 28 mm × 6.3 mm × 1.0 mm. Before deformation the specimens were polished to a mirror finish. Uniaxial tensile deformation was provided by a small portable tensile stage, which can be mounted in a white light reflection confocal microscope. Because of its high lateral and axial resolution, a confocal microscope is an ideal instrument to acquire topographic information of larger surfaces. Using a 20× objective lens, an area of 700 μm × 660 μm can be scanned with an axial resolution of 40 nm. The samples were mounted as flat as possible using an adjustable base plate, in order to use the smallest possible z step during the height measurements. The crosshead speed of the tensile stage was set at 10 μm/s, corresponding to a strain rate of 3.6×10^{-4}/s.

During the experiments the tensile stage was halted at a number of strains and confocal images were acquired at three positions. Care was taken to ensure that those positions were the same at every measurement in order to be able to study accurately the local roughness evolution with increasing strain. The measured height images were leveled before analysis, subtracting the best fitting first-order plane. Information about the crystal orientation was acquired using an OIM system mounted in a Philips XL30s field emission gun scanning electron microscope.

2.3. Data analysis

To analyze the surface morphology, we extracted roughness parameters from height–height correlation functions, assuming a partially self-affine scaling behavior [1,17,18]. The height–height correlation function applied to a matrix of digitized height values takes the form

$$g(p) = \frac{1}{N_y(N_x - p)} \sum_{l=1}^{N_y} \sum_{n=1}^{N_x - p} [h(p+n, l) - h(n, l)]^2, \tag{2}$$

where N_x and N_y are the dimensions of the height matrix. The correlations were calculated in one direction and averaged over the other.

Assuming a self-affine scaling behavior, then

$$h(x) \sim b^{-\alpha} h(bx), \tag{3}$$

where b is a constant and α is the scaling or Hurst exponent, provides a very useful set of parameters to characterize the surface. The height–height correlation function of a self-affine surface takes the form

$$g(r) = 2w^2 f(r/\xi), \tag{4}$$

where w is the rms width of the height distribution and $f(x)$ is a function that takes the following values:

$$f(x) = x^{2\alpha} \tag{5}$$

for $x \ll 1$ and $f(x) = 1$ for $x \gg 1$. For the height–height correlation function this means

$$g(r) = mr^{2\alpha} \tag{6}$$

for $r \ll \xi$ and

$$g(r) = 2w^2 \tag{7}$$

for $r \gg \xi$ with $m = 2w^2/\xi^{2\alpha}$. Therefore, plotting the correlation function (Eq. (2)) of a self-affine surface on a double logarithmic scale will result in a straight line with slope 2α until r is of the order of ξ. At larger values of r, the function will take a constant value of $2w^2$. To maintain good statistics, correlations were calculated for points with a separation up to 75% of the total profile length.

The heights of points at distances smaller than ξ are correlated, whereas points further apart are uncorrelated. Hence, the parameter ξ is called the correlation length. The scaling parameter α is a measure of this correlation. If the roughness is a result of a random walk displacement, α will be 0.5. Values of α larger than 0.5 indicate a positive correlation, whereas values smaller than 0.5 mean that the heights are anti-correlated.

The height images generated by the confocal microscope were flattened before the correlation function was calculated. The leveling applied does not interfere with the discussion and conclusions presented because the sample surface did not show any evidence of structures with a characteristic length between the correlation length shown in the results and the sample size. Therefore, only the macroscopic tilt of the sample was removed.

The correlation function $g(p)$, i.e. the average of the correlation functions of the individual lines, was then plotted on a double logarithmic scale and fitted to the self-affine approximation (Eq. (4)). A linear fit to the first section of the correlation function was used to determine the scaling exponent α. The rms value w was calculated directly from the height data. Finally, the correlation length ξ was determined from the intersection of a straight line with slope 2α through the first part of the correlation curve and the horizontal line $g(r) = 2w^2$. The resulting three parameters, α, ξ and w, completely describe the statistical morphology of the surface within the experimental limits set by the resolution of the confocal microscope. Within our work, we focus on the dependence of these parameters with increasing strain and examine the influence of the crystal structure and grain orientation.

Alongside information about the grain size and the texture of the material, OIM scans were used to determine the susceptibility of the grain to deformation. This 'hardness' is expressed as the Schmid factor m ($m = \cos\varphi\cos\lambda$ where φ is the angle between the applied force and the slip plane normal and λ the angle between the force and the slip direction). The slip system for which m is plotted is always the slip system with the highest Schmid factor. Finally, OIM was used to get an estimate of the deformation inside an

individual grain by calculating the grain orientation spread, which is the standard deviation of all orientations within the grain.

3. Results

Height–height correlation graphs are shown in Fig. 2 for a selected number of strain values. The higher-valued curves correspond to higher values of strain. The correspondence with the curve expected for partially self-affine behavior is good. Initially the points lie on a straight line and for large distances correlation is lost. This is especially true for the aluminum and zinc specimens. For the iron specimen the curves at lower strains are not as straight. Looking at the bottom curve ($\varepsilon = 0$), it appears that a correlation is present between points less than a few micrometers apart. This correlation, which is probably a result of the polishing, only slowly disappears with increasing amounts of strain.

It should be noted that for the zinc specimen, the curves are not shown for all strain values. Above a strain of $\varepsilon = 0.1$, the surface became too rough for the confocal microscope to make a scan of the full area. Crevices appear which reflect no light. Although the number of bad points is never higher than a few per cent of the total number of pixels, this has a large influence on the first section of the correlation graphs. To find out if ignoring of the bad points is justified, a good scan was recalculated with the omission of a few percent of its lowest points. The change in the correlation graph is significant. Hence the decision was made to ignore the measurements at strains $\varepsilon > 0.1$ for the calculation of the roughness exponent α and the correlation length ξ. However, the effect on the rms roughness w is negligibly small. Therefore, these values are included in Fig. 3, which shows an increase of w with increasing strain for the iron, zinc and one of the aluminum specimens.

In Fig. 4 a similar graph is shown for two aluminum specimens, which underwent exactly the same heat treatment (10 min at 450 °C, grain size 68 μm). The only difference is the thickness of the tensile specimens. One was polished to a thickness of 1.0 mm and the other was ground down to a thickness of 0.3 mm. The thicker tensile specimen roughens considerably more than the thinner one.

A linear fit was made to the first five points in every height–height correlation graph to obtain values for the scaling exponent α. In our previous paper [1] it was reported that for the aluminum specimens, the α-values increased upon straining until they saturated at values close to or even slightly above 0.9. In Fig. 5 the fitted α-values for iron and zinc are plotted. They show a similar increase at

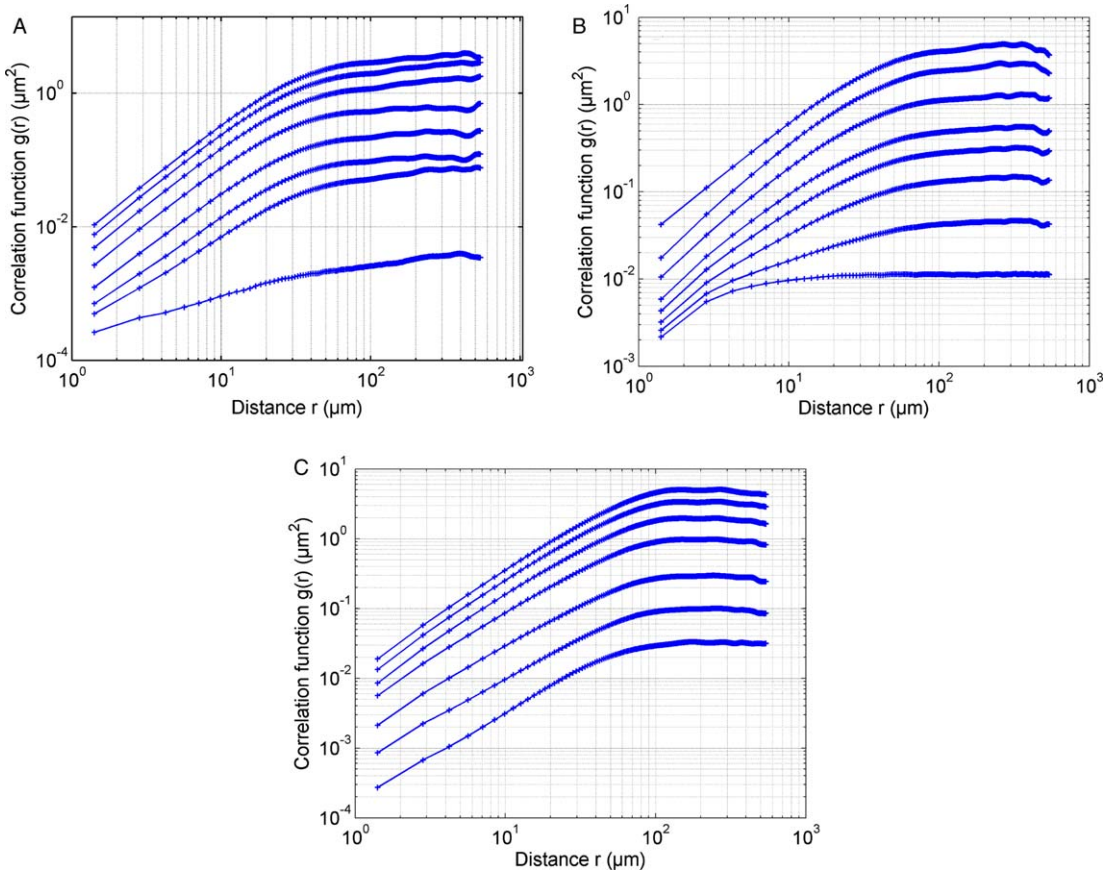

Fig. 2. Height–height correlation graphs for (A) aluminum sample with smallest grain size (31 μm) for strain values between $\varepsilon = 0$ and 0.22, (B) iron sample between $\varepsilon = 0$ and 0.19 and (C) zinc sample for strains between $\varepsilon = 0$ and 0.10.

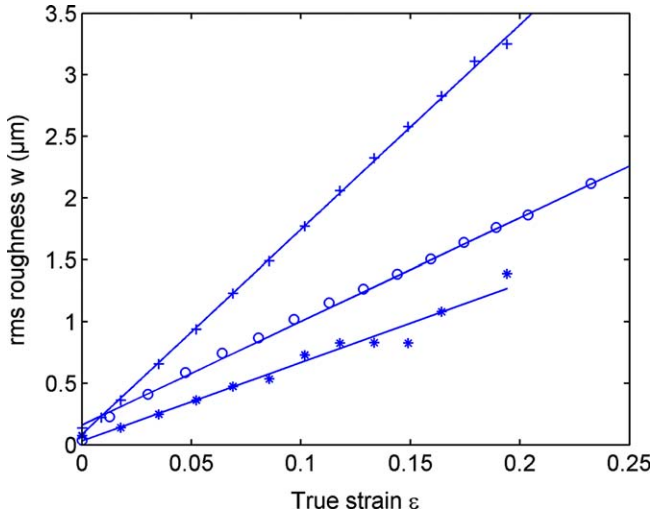

Fig. 3. Rms roughness plotted versus true strain: ∗, iron sample; ○, aluminum sample with grain size 44 μm; +, zinc sample.

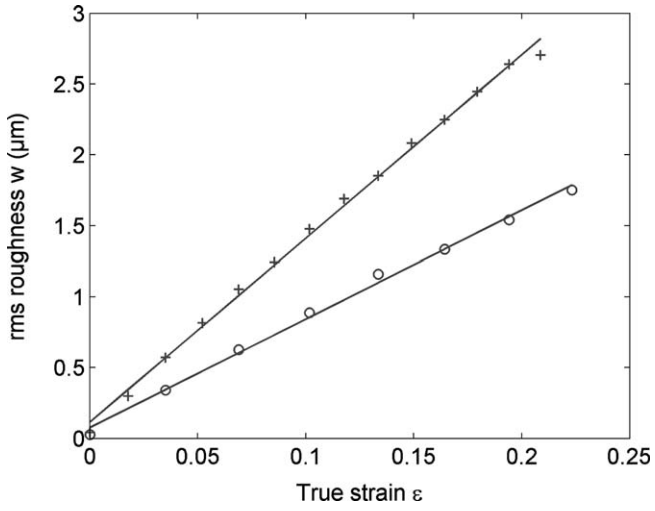

Fig. 4. Rms roughness versus true strain plot for two aluminum specimens with similar grain size (68 μm) but with different thickness: ○, 300 μm thick; +, 1.0 mm thick.

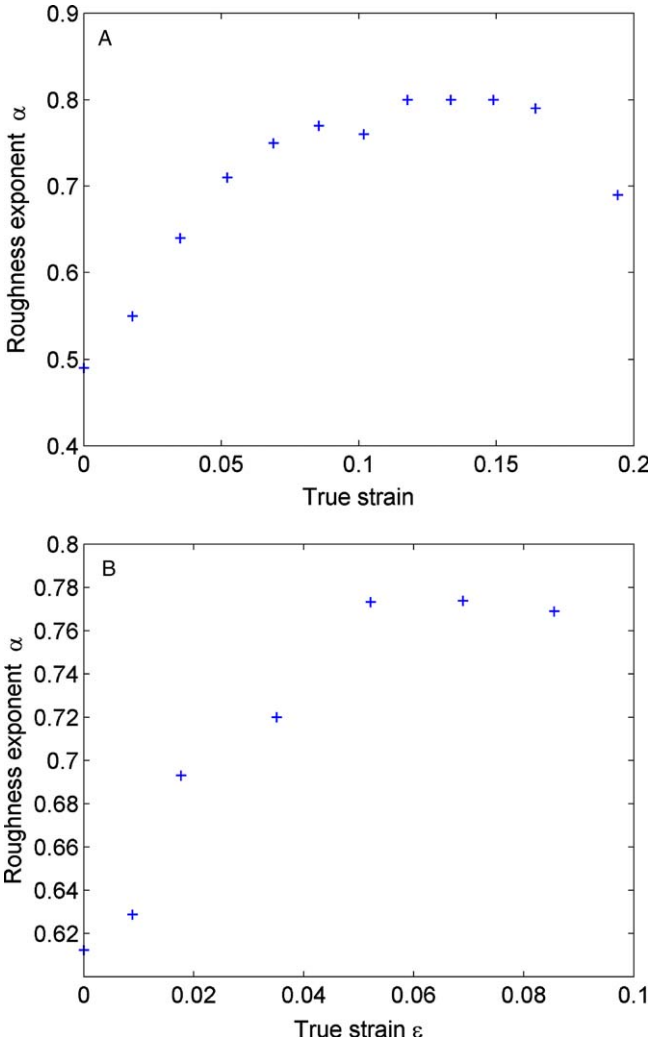

Fig. 5. Fitted values for the roughness exponent α: (A) iron specimen; (B) zinc specimen.

low strains but saturate at much lower values. Fig. 5A shows a plateau for strains in between 0.12 and 0.16 of $\alpha = 0.80$ but the final value at a true strain of 0.19 is much lower: $\alpha = 0.69$. For the zinc specimen measurements, the values appear comparable. Unfortunately, only α-values for low strains could be calculated as explained above.

Calculations of the correlation length ξ for the iron and zinc specimens show that it is of the same order of magnitude as the grain size, as is also found for aluminum [1]. Averaging ξ-values for the last five iron curves yields a value of $\xi = 20$ μm and averaging all results for zinc yields $\xi = 44$ μm. Both values are slightly below the grain size.

Since all topographic measurements are performed on the same position, it is possible to examine the roughness evolution with increasing strain. This is done in Fig. 6 for iron. Fig. 7 shows the relation between the orientation of

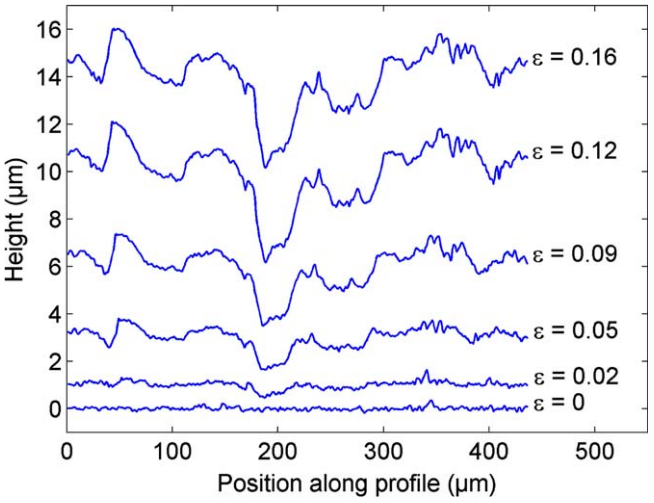

Fig. 6. Confocal height profiles measured on the same place on the iron sample for increasing strain values.

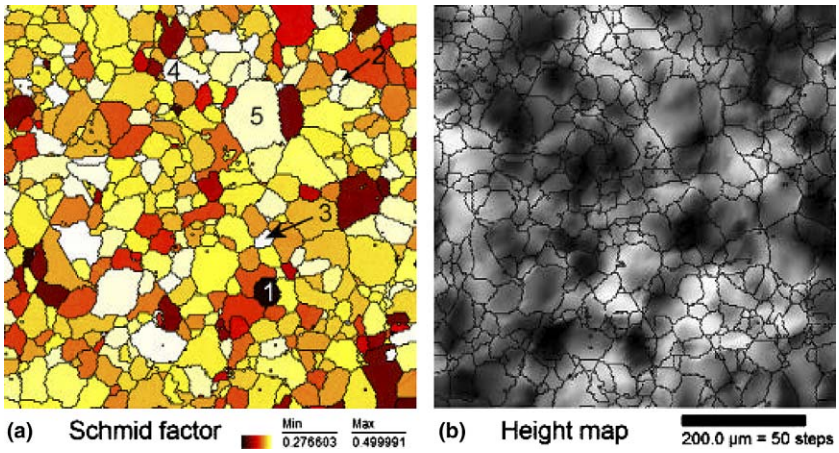

Fig. 7. Comparison between (a) the initial Schmid factor and (b) the height map on the same position after 10% tensile deformation. The scale in (a) runs from black for low values to white for the highest Schmid factors. The sample is aluminum with a grain size of 30 μm. The overlay in (b) showing the grain boundaries is taken from an OIM scan of the deformed specimen.

the surface grains and the topography resulting from a considerable amount of tensile deformation. These measurements were performed on an aluminum sample with an average grain size of 31 μm. Fig. 7(a) shows an OIM map from an area before deformation started. Plotted is the Schmid factor of the grains as a measure of their hardness. In Fig. 7(b) the confocal height map is shown of the same area after 10% deformation. The black areas correspond to the lowest points on the surface and the white regions to the highest points. The overlay is taken from an OIM scan performed after the deformation and shows the grain boundaries dividing grains with orientation differences over 5%. The same scan is used to plot the grain orientation spread as a function of the Schmid factor in Fig. 8. Finally in Fig. 9(a), a Schmid factor plot is shown of an aluminum sample with 90 μm grains in cross-section. This sample was deformed 20% after which a confocal height map was made and the sample was ground from the side to reveal the grains responsible for the roughness profile (Fig. 9(c)).

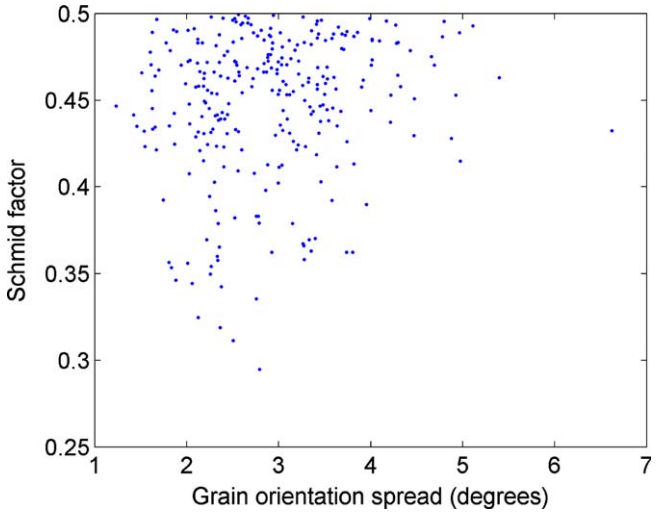

Fig. 8. Schmid factor plotted as a function of the grain orientation spread for the same aluminum sample as used in Fig. 7 after 10% straining.

4. Discussion

In our previous work [1], we concluded that our statistical analysis offers more insight into the nature of the roughness than most common techniques. This is especially true when the roughness characteristics change on different length scales, as is the case for polycrystalline metals. We showed that for polycrystalline aluminum, the rms roughness increased linearly with both strain and grain size. In fact, on length scales above the correlation length, which was shown to be closely related to the grain size, the shape of the roughness profiles did not change upon straining. The surface topography at high strain is to a close approximation simply a vertically rescaled replica of the topography at the same position at lower strains. This becomes all the more striking if one considers that on a subgrain scale the aluminum surface remains nearly flat, as is indicated by the high values of the roughness exponent α ($\sim$0.9). Fig. 2 shows that characterization of the surface roughness using the parameters α, ξ and w is also justified for the iron and zinc specimens. The curves initially show a linear correlation behavior indicative of self-affine scaling on smaller length scales. For points farther apart, this correlation disappears completely, resulting in a horizontal tail in the graph.

All three curves in Fig. 3 are remarkably straight. The linear relationship between the rms roughness w and strain holds for all three materials. Since the geometry of the three tensile specimens is exactly the same and assuming that the linear relationship between rms roughness and grain size also holds for iron and zinc, one can divide the slope of the curves by the grain size and calculate the constant c in the following equation:

$$w = c \cdot \bar{d} \cdot \varepsilon. \tag{8}$$

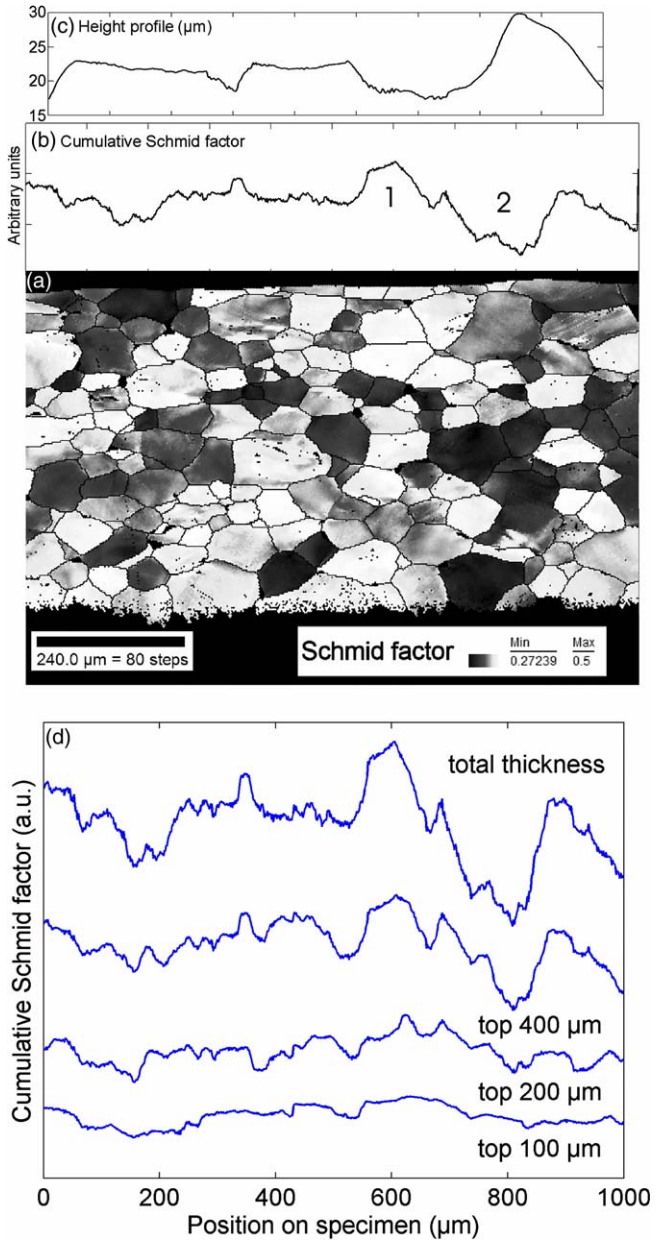

Fig. 9. Cumulative Schmid factor across the thickness of the specimen appears to be related to the roughness on the surface. (a) Schmid factor on the cross-section of a deformed aluminum sample with a grain size of 90 μm. The scale runs from black for low values to white for the highest Schmid factors. (b) The cumulative Schmid factor summing across the thickness. (c) The height profile on the surface. (d) The Schmid factor summed over slices of varying thickness of the specimen.

For aluminum this yields $c = 0.19$, for iron $c = 0.20$ and for zinc $c = 0.32$. The zinc specimen becomes much rougher than aluminum and iron for comparable strains and grain sizes. The iron and aluminum behave quite similar. An explanation for this difference is found when looking at the possible number of slip system responsible for the plastic deformation in these materials. In fcc aluminum, there are 12 independent $\{1\,1\,1\}\langle 1\,1\,0\rangle$ slip systems. For bcc iron the number of slip systems is less trivial, because slip occurs not only on the close-packed $\{1\,1\,0\}$ planes, but also on the $\{1\,1\,2\}$ planes (sometimes even on $\{1\,2\,3\}$). Since slip occurs in the close-packed $\langle 1\,1\,1\rangle$ directions, there are 12 independent combinations of $\{1\,1\,0\}$ slip planes and slip directions. The same number of independent combinations is found for the $\{1\,1\,2\}\langle 1\,1\,1\rangle$ system. Plastic deformation of bcc metals in general exhibits characteristic features depending on the deformation temperature, e.g. a strong temperature dependence of the yield stress and anomalous slip. The choice of slip system is temperature dependent. At low temperatures the $1/2a_0\langle 1\,1\,1\rangle$ screw dislocation is in its 'ground state', its core having a threefold screw symmetry, which will allow slip on $\{1\,1\,0\}$ planes. At elevated temperatures however, the dislocation will enter a metastable 'excited state'. The core configuration is now such that slip on $\{1\,1\,2\}$ planes is allowed. The temperature at which this first-order phase transition occurs is approximately 100 K, making the $\{1\,1\,2\}$ planes the dominant slip planes at room temperature [10,11]. In the past, in situ experiments have been performed [19–21] at low and intermediate temperatures on Nb, Mo and bcc Fe. In all these bcc materials a transition has been observed in the dislocation dynamics between a low-temperature behavior, characterized by an almost continuous movement of long screw dislocations, and an intermediate-temperature behavior, where mixed dislocations predominate.

In zinc, which has a hexagonal crystal structure, slip is primarily confined to the basal planes. There are only three basal $(0\,0\,0\,1)\langle 1\,1\bar{2}\,0\rangle$ slip systems available, two of which are independent. Taylor pointed out that for a polycrystalline material to undergo a homogeneous deformation without cracking, at least five independent slip systems must be present [12]. Other probable deformation modes are the first-order prism and pyramidal planes, i.e. $\{1\bar{1}\,0\,0\}\langle 1\,1\bar{2}\,0\rangle$ and $\{1\bar{1}\,0\,1\}\langle 1\,1\bar{2}\,0\rangle$, respectively. However, also second-order pyramidal slip $\{1\,1\bar{2}\,2\}\langle 1\,1\bar{2}\,\bar{3}\rangle$ has been observed in zinc [13,14]. Furthermore, deformation twinning is common in hcp metals, with for zinc only the most common $\{1\,0\bar{1}\,2\}$ twins being active [15].

The point to be made here is that when two randomly oriented grains are observed, on average the difference in their hardness, i.e. the difference in the shear stress resolved on the primary slip system, will be higher for zinc, while this difference will be approximately equal for aluminum and iron. The roughness is believed to originate as a result of these kinds of hardness differences between neighboring grains. Softer grains, i.e. grains with a higher stress resolved on the primary slip system, will have a tendency to deform more than the harder grains. They are restrained, however, by the neighboring grains. These strain incompatibilities may lead to an inhomogeneous rotational deformation in the grain and subsequently also in a part of the surrounding grains. An attempt to model a simple system consisting of harder and softer grain was made by Zhao et al. [16]. Since the number of available slip systems in the zinc is limited, the average differences in hardness between the grains will be higher for non-textured materials. The higher straining discrepancies will lead to a

rougher surface. As long as the hardness differences between the grains do not change significantly, and their elongation due to the tensile deformation is well below the grain size, the total deformation of the grain assembly will be more or less constant, explaining the linear increase of the rms roughness w with strain (Fig. 3, Eq. (8)) and also the constant shape of the roughness profiles (Fig. 6).

For all the specimens, the clear distinction in correlation behavior is present between the two regimes, separated by the correlation length ξ, which for each material is approximately equal to the grain size. Below the correlation length, the roughness is no longer described by the rms roughness but rather by the exponent α. The values obtained for α from the correlation graphs show that both iron and zinc are much rougher than the aluminum with its nearly flat facets. An explanation for this fairly large difference in small-scale roughness is the formation of dislocation structures inside the grain, typical of aluminum. These screw dislocations assemble in cell walls and eventually in more ordered subgrain boundaries. These structures, with a typical size of 0.5–2 μm, relax the stresses inside the material and may therefore also reduce the amount of roughness features observed on the surface, which effectively leads to a more positive correlation between neighboring points on the surface.

In a simplified analysis, one might say that the surface roughness is mainly due to the different deformation of surface grains. Softer grains will deform more easily, stretch and cause a local depression on the surface. However, if this explanation is valid, the two curves in Fig. 4 should not differ as much as they do. The top 150 μm in both specimens are comparable. Since the grain size in these specimens is 68 μm, this amounts to at least the two top layers of grains. Still, upon straining, the roughness developing on the surface of the thicker specimen is much larger than the roughness on the thinner specimen. Clearly more grains should be taken into account than just the first couple of top layers.

Figs. 7 and 8 demonstrate the importance (or lack of importance) of the surface grains on the roughness. For some grains the topography can be understood when looking at the grain orientation. Grain number 1 in Fig. 7(a) is the grain with the lowest Schmid factor. This very hard grain deforms only a little and corresponds to one of the highest points on the surface as can be observed from Fig. 7(b). The grains in Section 2 and grain number 3 show the opposite relation. They have a Schmid factor close to the maximum of 0.5 and will easily deform, when allowed for by other grains. Their deformation causes local depressions on the sample surface. However, these correlations are only incidental. Grain number 4 for example has a low Schmid factor but lies on a ridge on the surface. The overlay in Fig. 7(b), indicating the grain boundaries, does not overlap with local minima or maxima in the height map, nor can the Schmid factor explain the multiple peaks and valleys present on the surface of grain number 5.

At a first glance Fig. 8 looks perhaps rather arbitrary. There are some comments to be made about the quantities used in this figure. The Schmid factor does not completely describe the susceptibility of the grain to plastic deformation, since it only focuses on the primary slip system. Also the grain orientation spread does not bear a one-to-one relation with the amount of deformation in the grain. Not only will the larger grain probably have a higher spread in orientation, which is then not related to the orientation of the grain, but there is also the problem that only deformation leading to a rotation of a part of the grain will cause the orientation spread to increase. Normal slip of course does not change the orientation of the lattice. Fig. 8 shows that it is not justified to assume that the softer surface grains (i.e. those grains with a high Schmid factor) automatically deform the most. All the points are clustered in the top left corner of the graph, indicating that the grains must have a suitable orientation for a high deformation to occur. However, the opposite is not true and some grains with a high Schmid factor are seen to deform only a little.

From the fractal analysis of the surface roughness it appears that there is no correlation of the vertical movement at the surface between points further apart than roughly the mean grain size $\bar{d}$. Therefore, it seems reasonable to look for a correlation with the structure beneath the surface. Fig. 9(b) shows that when the Schmid factors at all positions of the cross-section below a point are summed, there is a correspondence with the surface height profile. If the cumulative Schmid factor across a certain section of the specimen is high, that section will stretch easily without much hindrance. This will lead to a depression on the surface as can be seen in region 1. In region 2 the opposite occurs. On average there are many hard grains here that will deform less. The height profile consequently shows a higher region at these points. As can be seen from the different curves in Fig. 9(d), the correspondence is only present when the summation of the Schmid factors is performed across the entire thickness of the specimen.

For thick samples without texture, the absolute differences in cumulative Schmid factor from position to position will be larger than for thin samples. This is evident from Fig. 9(d) and is consistent with the results of Fig. 4 that show a higher rms roughness for a thick sample than for a thin sample of the same material.

5. Conclusions

It has been shown that the statistical description of a rough polycrystalline metal surface in terms of the rms roughness w, the scaling exponent α and a correlation length ξ can be applied to metal systems with strongly varying crystal structures. It helps to identify two different regimes of roughening. On a subgrain scale the roughening is self-affine with roughness exponents of 0.9 for aluminum but 0.8 for iron and zinc. On a multiple grain scale there is no correlation between different points and the surface can be described by an rms roughness, which increases linearly

with increasing strain. These experiments suggest that local hardness differences between the grains are responsible for this roughening. The limited number of available slip systems in zinc causes on average larger differences in hardness between neighboring grains. Hence, zinc roughens more than aluminum and iron.

The experimental OIM results presented justify the conclusion that the roughness is determined by multiple layers of grains rather than just by the surface grains, and in particular it is hypothesized that the spatial variation of the cumulative Schmid factor (determined along a column below a certain point) determines the local surface heights.

Acknowledgments

The work is part of the research program of the Foundation of Fundamental Research on Matter (FOM, Utrecht) and has been made possible by financial support from the Netherlands Organization for Research (NOW, The Hague), the Netherlands Institute for Metals Research, the Foundation for Technical Sciences and the Innovative Research Program (IOP-Senter, The Hague).

References

[1] Wouters O, Vellinga WP, van Tijum R, De Hosson JThM. Acta Mater 2005;53:4043.
[2] Lee PS, Piehler HR, Adams BL, Jarvis G, Hampel H, Rollett AD. J Mater Proc Technol 1998;80–81:315.
[3] Becker R. Acta Mater 1998;46:1385.
[4] Wittridge NJ, Knutsen RD. Mater Sci Eng A 1999;269:205.
[5] Raabe D, Sachtleber M, Weiland H, Scheele G, Zhao Z. Acta Mater 2003;51:1539.
[6] Wilson DV, Roberts WT, Rodrigues PMB. Metall Trans A 1981;12:1603.
[7] Baczynski GJ, Guzzo R, Ball MD, Lloyd DJ. Acta Mater 2000;48:3361.
[8] Mahmudi R, Mehdizadeh M. J Mater Proc Technol 1989;80–81:707.
[9] Wilson DV, Roberts WT, Rodrigues PMB. Metall Trans A 1981;12:1595.
[10] Seeger A, Wasserbäch W. Phys Stat Sol (a) 2002;89:27.
[11] Seeger A. Phys Stat Sol (a) 2004;201:R21.
[12] Taylor GI. J Inst Met 1938;62:307.
[13] Yoo MH, Wei CT. J Appl Phys 1967;38:4317.
[14] Blish RC, Vreeland T. J Appl Phys 1969;40:884.
[15] Yoo MH. Metall Trans A 1981;12:409.
[16] Zhao Z, Radopvitzky R, Cuitino A. Acta Mater 2004;52:5791.
[17] Zaiser M, Madani F, Koutsos V, Aifantes EC. Phys Rev Lett 2004;93:195507.
[18] Zhao Y, Wang GC, Lu TM. Characterization of amorphous and crystalline rough surface: principles and applications. New York: Academic Press; 2001.
[19] Matsui H, Saka H, Noda K, Kimura H, Imura. Scr Metall 1974;8:467. 1976;10:59.
[20] Louchet F, Kubin LP, Vesely D. Philos Mag A 1979;39:433.
[21] Christian A, Kanert O, De Hosson JTM. Acta Metall 1990;38:2479.